

Towards a spatio-temporal atlas of 3D cellular parameters during leaf morphogenesis

F. Selka¹, T. Blein², J. Burguet¹, E. Biot¹, P. Laufs¹ and P. Andrey¹

¹ Institut Jean-Pierre Bourgin INRA, AgroParisTech, CNRS, Université Paris-Saclay, F-78000 Versailles, France

² Institut des Plantes Paris-Saclay, Gif-sur-Yvette, France

selka.faical@gmail.com

Abstract

Morphogenesis is a complex process that integrates several mechanisms from the molecular to the organ scales. In plants, division and growth are the two fundamental cellular mechanisms that drive morphogenesis. However, little is known about how these mechanisms are coordinated to establish functional tissue structure. A fundamental bottleneck is the current lack of techniques to systematically quantify the spatio-temporal evolution of 3D cell morphology during organ growth. Using leaf development as a relevant and challenging model to study morphogenesis, we developed a computational framework for cell analysis and quantification from 3D images and for the generation of 3D cell shape atlas. A remarkable feature of leaf morphogenesis being the formation of a laminar-like structure, we propose to automatically separate the cells corresponding to the leaf sides in the segmented leaves, by applying a clustering algorithm. The performance of the proposed pipeline was experimentally assessed on a dataset of 46 leaves in an early developmental state.

1. Introduction

A challenging task in plant developmental biology is to understand how a few cells can give rise to complex structures such as leaves. Because of the presence of a cellular wall, plant morphogenesis essentially results from cell division, growth and elongation. However, the coordination between these mechanisms at the whole leaf scale remains largely unknown [7]. Imaging protocols have been developed to monitor morphological changes at the cellular level [3, 8] and image analysis has been used to quantify spatial and temporal growth patterns of cells on the basis of morphological features [4]. In particular, the geometric properties (size, shape) of segmented cells have been analyzed [6, 5]. A popular approach is to track growth of plant organs using 2D and 2.5D images (curved surfaces). Elsner *et al.*

[6] proposed to track growth on 2D images where a sample of leaf cells was analyzed. Barbier de Reuille *et al.* [5] relied on intensity projections on curved surfaces to obtain a clear outline of the cell morphology in simple plant organs like the shoot apical meristem that can be assimilated to essentially 2D structures. In [12], the authors investigated a computational approach to generate 3D cellular atlases based on an automatic cell type identification within 3D images of radially symmetric plant organs like roots. However, leaves are asymmetric, dome-shaped with a complex structure and organization of cells. To tackle this complexity, cell morphology must be analyzed in 3D and take into account the entire spatial cell organization.

Leaves have two different epidermal cell populations, the adaxial (upper) and abaxial (lower) ones. The differences in gene expression between both sides play an important role in cell differentiation pattern and leaf growth [13]. To date, no quantitative analysis has been performed to quantify the difference between abaxial and adaxial populations in terms of cell morphology. Only a visual assessment of a sample of leaf cells was provided [9, 13, 16] which is tedious and user dependent. Thus, cell morphology must be characterized automatically regarding the leaf sides in order to properly quantify shape features during leaf growth.

In this paper, we propose a comprehensive pipeline for analyzing and quantifying epidermal cell morphology during leaf development. Our strategy relies on a robust and automated 3D cell shape spatial distribution analysis, and also includes an approach to separate the adaxial and abaxial cell populations. For each epidermal cell, several shape properties are measured, resulting in building a spatio-temporal atlas of epidermal cell morphologies during leaf morphogenesis. Therewith, systematic maps of cell geometrical properties are generated over the whole leaf surface. These surface maps can then be visualized in a 3D viewer to reveal domains with distinct characteristics.

The paper is organized as follows. In Sec. 2, we describe the methodology used to generate the data. The methods for the 3D cell shape analysis are presented in Sec. 3. The

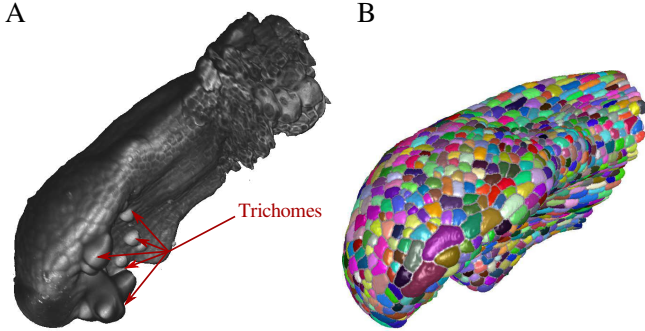


Figure 1: Acquired and processed 3D leaf images. (A) Volume rendering of a 3D confocal image of a leaf with stained cellular walls. (B) Result of the segmentation of epidermal cells, visualized using the *Sviewer* software [2].

results are shown in Sec. 4. Finally, the relevance of our proposed strategy is discussed and conclusions are proposed in Sec. 5.

2. Image data

In this work, leaves were extracted from different shoot apical meristems of *Arabidopsis thaliana Col-0* plants. Leaves were fixed, stained and imaged using a confocal microscope according to the protocol described in [18] to highlight cell walls, thus providing a clear cell boundary for segmentation. The size of images (respectively width, height, depth) varied from $91 \times 94 \times 97$ voxels for the smallest leaf to $1263 \times 687 \times 309$ voxels for the largest one. Voxels were cubic with a size of $0.53 \times 0.53 \times 0.53 \mu\text{m}$. Fig. 1A shows an example of a volume rendering of a stained leaf. One disadvantage of using fixed leaves is that only static images can be analyzed. To address this issue, leaves were sampled at different stages of their development. Leaf length was used as a proxy of the developmental time and was measured manually as the distance between the bottom of the leaf blade and the leaf tip (Fig. 2B).

Images were automatically segmented using a 3D watershed algorithm. The segmentation process followed the method described in [15]. Briefly, a local intensity variance normalization was performed in order to alleviate attenuation and irregular staining effect. Also the contrast between cell walls and other regions was enhanced by applying an anisotropic filtering [19]. The segmentation results presented high accuracy and thus no post-processing was needed. An expert manually edited the segmented images to assign a single label to all sub-epidermal cells (Fig. 2B). Trichomes (leaf hairs; see arrows in Fig. 1A) which are huge differentiated cells, were manually removed from the segmented images. Fig. 1B shows an example of a segmented leaf after edition.

Our data-set was composed of 46 leaf images with

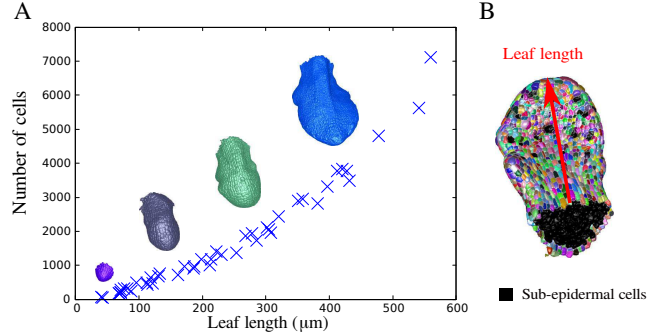


Figure 2: Distribution of leaf size in the data-set. (A) Number of epidermal cells as a function of leaf length. (B) Leaf length measurement.

lengths varying from $50 \mu\text{m}$ to $580 \mu\text{m}$, thus covering the early developmental stages. The number of epidermal cells per leaf varied from 40 to 7000. Fig. 2A plots the number of epidermal cells as a function of leaf length in the data-set. We noticed that estimating developmental time on the basis of the leaf length was consistent with regards to the number of cells.

3. 3D cell image analysis

In order to analyze morphological features of epidermal cells, we propose a variety of quantitative parameters which are related to cell and tissue growth, including size, shape and spatial organization, and that can be extracted from the 3D segmented images. Two types of cellular parameters can be measured in our pipeline. Firstly, we present the measurements that do not depend on the context (local environment in the organ) of the cell. These non-contextual measurements are similar to the parameters described in [1] to analyze the shape of animal and plant cell nuclei. Secondly, we propose parameters that depend on the relative positioning of each cell with regards to its immediate environment. Finally, we present a method for the separation of abaxial and adaxial cell populations. This classification will allow the comparison of the morphological parameters between the two leaf sides.

3.1. Non-contextual cell shape parameters

3.1.1 Sphericity

This classical parameter quantifies the similarity between a cell and a sphere and is defined as:

$$\Psi = 36\pi V^2/A^3 \quad (1)$$

where V and A are, respectively, the volume and the cell surface area. For a sphere, $\Psi \simeq 1$ and Ψ decreases when the shape becomes more elongated or irregular.

3.1.2 Elongation

Cell elongation was measured based on the ratio of the first two eigenvalues of the cell inertia matrix:

$$E = \sqrt{\lambda_1/\lambda_2} \quad (2)$$

where λ_1 (major axis) and λ_2 (intermediate axis) are the first two eigenvalues of the inertia matrix.

3.1.3 Flatness

The flatness was quantified based on the ratio of the last two eigenvalues of the inertia matrix:

$$F = \sqrt{\lambda_2/\lambda_3} \quad (3)$$

where λ_2 (intermediate axis) and λ_3 (minor axis) are the last two eigenvalues of the inertia matrix.

3.2. Contextual cell shape parameters

3.2.1 Thickness

Leaf thickness has been investigated in studies of leaf expansion [20, 17]. There, manual 2D measurements under a light microscope [17] or on an orthogonal view of images acquired using confocal microscopes [20] were performed. In the present work, we introduce an automatic measure of the Epidermal Cell Thickness (ECT), defined for each epidermal cell as the distance between the sub-epidermal tissue and the leaf external surface.

Many approaches have been proposed to estimate the local thickness of complex 3D objects. In [14], a local maximum diameter which fits the 3D objects along the medial axis was used. More recently in [21], the classic erosion thickness measurement over the medial axes of 2D shapes [10] was generalized in 3D. Although both approaches show robust results for the local thickness estimation of 3D objects, they are not adapted to measure ECT. Indeed, ECT is defined by considering the extension of the cell relatively to the local orientation of the leaf surface. For the same reason, ECT cannot be measured using the principal axis of inertia of the cell. For example, in Fig. 3A, two cells with the same ECT are shown. On the left, the ECT corresponds to the smallest axis, while on the right, it corresponds to the largest one.

We propose to calculate ECT with respect to the position of the sub-epidermal cells. Let B_s be the barycenter of the patch of cell surface that is in contact with the sub-epidermal cells and let B_c be the barycenter of the cell. The surface of contact used to compute B_s corresponds to the coordinates of the cell voxels that are neighbors to voxels with sub-epidermal label within a $3 \times 3 \times 3$ neighborhood. Let \vec{N}_t be the thickness direction vector defined as the unit direction vector of the $\vec{B}_s\vec{B}_c$ line (Fig. 3B). Let S_c be the

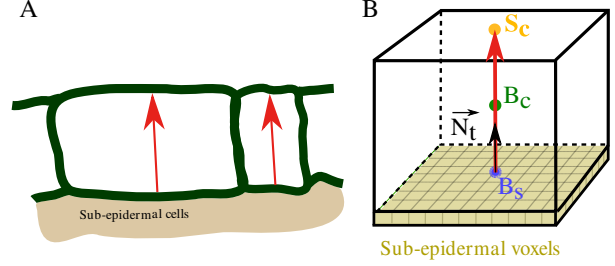


Figure 3: Epidermal cell thickness. (A) Epidermal cell thickness direction. (B) Calculation of the thickness direction vector \vec{N}_t and the ECT.

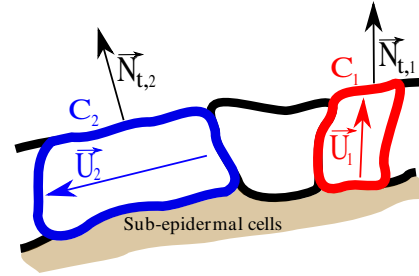


Figure 4: Measuring cell orientation with regards to local leaf surface.

intersection point between the line spanned by \vec{N}_t and the external cell surface. The ECT is defined as $\|\vec{B}_s\vec{S}_c\|$. Note that \vec{N}_t can be used as an approximation of the leaf surface normal vector.

3.2.2 Cell orientation

Cell division and differential growth are cellular processes that occur during leaf growth. In particular, cell orientation can be interpreted in terms of local growth orientation. In this paper, we propose a measurement of the cell orientation based on the normal vector \vec{N}_t and the first principal axis of the cell \vec{U} . The relative cell orientation was measured as:

$$O = |\vec{U} \cdot \vec{N}_t| \quad (4)$$

For example, let us for instance consider two cells C_1 and C_2 with distinct orientations (see Fig. 4). Let $\vec{N}_{t,1}$ and $\vec{N}_{t,2}$ be the estimates of the leaf surface normals for C_1 and C_2 , respectively. Let \vec{U}_1 and \vec{U}_2 be the major axis vectors of C_1 and C_2 , respectively. The absolute value of the scalar product $|\vec{U}_1 \cdot \vec{N}_{t,1}| \simeq 1$ indicates that C_1 is oriented perpendicularly to the leaf surface. Conversely, $|\vec{U}_2 \cdot \vec{N}_{t,2}| \simeq 0$ indicates that C_2 is elongated along the parallel direction to the surface.

We set a threshold on the scalar product absolute value at $\frac{\sqrt{2}}{2}$ (corresponding to an angle 45°) in order to separate

cells in two groups: collinear (above threshold) and perpendicular (below threshold) to the leaf surface.

3.3. Separation of the abaxial and the adaxial sides

Leaves develop distinct upper and lower surfaces that are known to have different characteristics. This raises the question whether the two cell populations of the abaxial and adaxial sides exhibit differences in their geometrical properties. In turn, this leads to the problem of automatically separating these two populations.

3.3.1 Automatic leaf side separation

We propose to automatically separate the cells from the two sides in the segmented leaves by applying a clustering algorithm to the set of normal vectors $\{\vec{N}_{t,i}\}$. Fig. 5 summarizes the proposed approach and provides an example of cell partition. From a segmented image we compute the normal vectors $\{\vec{N}_{t,i}\}$ of cells that indicate, as shown in Fig. 5, their orientations with respect to the sub-epidermal cells. In this example, we display the normalized $\{\vec{N}_{t,i}\}$ vectors in a common 3D coordinate system. Applying the K-means algorithm to classify vectors in two clusters, one can clearly see that the vectors are separated in two distinct groups regarding their main orientations and that the two groups correspond to the two leaf sides.

3.3.2 Validation of the method

In order to validate the proposed method for the separation of the abaxial and adaxial cell populations, we asked four biologist experts to define the margin of the abaxial and adaxial cells by manually annotating cells. The experts independently labeled the margins of 6 leaves using the *Sviewer* software [2]. They interactively oriented the surface of segmented leaves and marked the cells they considered to be at the abaxial and adaxial margins (respectively, red and green spheres in Fig. 6). Considering this margin annotation, we assigned all unmarked cells to either abaxial or adaxial sides (in practical, by propagating the expert margin annotations from cell to cell). For each expert, we obtained two distinct groups of cells corresponding to the separation of the two sides (turquoise and orange cells in Fig. 6). The annotation provided by each expert was used in turn as a ground truth to which the results of our classification algorithm and the annotation of the other experts were compared. The ratio of incorrectly labeled cells was computed as:

$$Err = \frac{|X_i \neq Y_i|}{|X_i|} \quad (5)$$

where $X_i = \begin{cases} abaxial \\ or \\ adaxial \end{cases}$ and $Y_i = \begin{cases} abaxial \\ or \\ adaxial \end{cases}$ are, respectively, ground truth expert cell annotations and the cell labels defined by the algorithm or another expert. For each incorrect cell we also measured a cell distance which corresponds to the number of cells separating it from the margin defined by the ground truth.

4. Results

We assess in this section the practical value of our proposed strategy for analyzing and quantifying cell morphology during leaf growth. Firstly, we give an overview of the quantifications that can be provided using our framework for leaf epidermal cell analysis. Secondly, we show that our proposed method for the separation of the abaxial and adaxial cell populations provide similar results as those provided by the annotation of the experts. Finally, we compare the difference in cell shape measurement between abaxial and adaxial sides.

4.1. Quantifications of leaf cell parameters

Thanks to our strategy, many possible analyses of cell parameters are possible. As an illustration, Fig. 7 shows a comprehensive map of epidermal cell thickness through the surface of an individual leaf. Parameter values are projected on a 3D surface extracted from a binary mask of the 3D volume image using the Marching Cubes algorithm [11] and displayed using a color look-up-table. Substantial variations of the ECT were observed throughout the leaf surface. More specifically, we noticed that the thickness was high at the leaf tip margin and along the central axis of the abaxial side and was low in tooth regions (blue squares in Fig. 7). We also noticed the presence of a cell with a high thickness in the tooth region (green square in Fig. 7) that will indubitably become a trichome. For each computed parameter, such a surface with projected values can be generated, thus providing a way to visualize and compare various cell shape parameters during leaf development.

Table 1 shows the average and standard deviation of the cell parameters computed on 8 leaves. These leaves were selected at different developmental steps to give a synthetic overview of the leaf spatio-temporal evolution. Firstly, we observed an increase of the ECT and cell volume, which is correlated with the increase of leaf length and number of cells. There was a globally decreasing trend of cell elongation with leaf length. However, we also observed that the maximal elongation value increased with leaf length, cell volume and ECT. For example, for leaf 4 the maximal values were: $E = 4.66$, $V = 1093.6 \mu\text{m}^3$, $ECT = 12.01 \mu\text{m}$; for leaf 8 the maximal values were: $E = 6.71$, $V = 7813.8 \mu\text{m}^3$, $ECT = 15.58 \mu\text{m}$. The increase of these parameters suggests that a group of cells

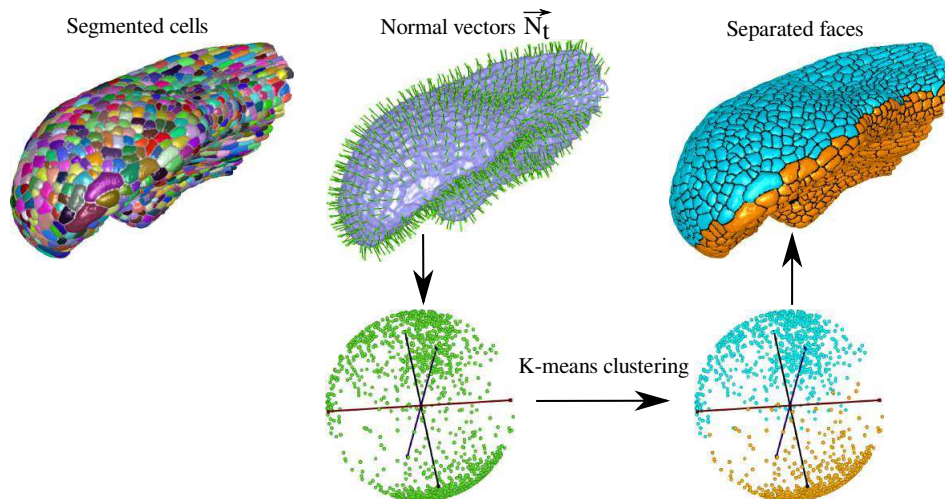


Figure 5: Separation of the adaxial and the abaxial sides based on clustering of thickness direction vectors.

Table 1: 3D morphological cell parameters (average \pm standard deviation)

Leaves	$L(\mu m)$	Cells	$V(\mu m^3)$	Ψ	E	F	$ECT(\mu m)$
1	41	69	151.61 ± 58.40	0.18 ± 0.02	1.54 ± 0.48	1.41 ± 0.24	5.26 ± 1.54
2	72	281	245.46 ± 129.21	0.20 ± 0.03	1.56 ± 0.44	1.24 ± 0.19	6.37 ± 1.44
3	133	764	245.49 ± 146.47	0.19 ± 0.03	1.41 ± 0.34	1.34 ± 0.25	6.79 ± 1.45
4	214	1172	267.68 ± 154.61	0.21 ± 0.04	1.43 ± 0.37	1.32 ± 0.23	6.94 ± 1.31
5	222	1400	293.56 ± 192.15	0.20 ± 0.03	1.42 ± 0.33	1.31 ± 0.24	7.43 ± 1.44
6	358	2953	292.14 ± 253.82	0.20 ± 0.03	1.36 ± 0.32	1.37 ± 0.26	7.85 ± 2.01
7	428	3781	333.10 ± 332.36	0.20 ± 0.04	1.41 ± 0.47	1.39 ± 0.27	8.24 ± 1.77
8	478	4797	329.70 ± 362.47	0.20 ± 0.03	1.37 ± 0.35	1.41 ± 0.28	8.20 ± 1.55

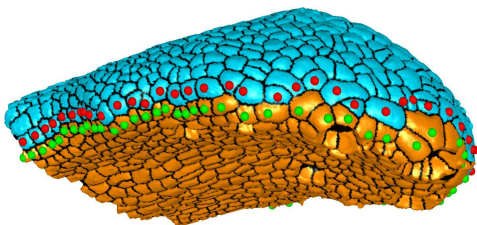


Figure 6: Example of manual annotation of one expert for the abaxial (*Red*) and adaxial (*Green*) margin cells, defining the unambiguous leaf side separation (*Turquoise*: abaxial side; *Orange*: adaxial side).

differentiate from the rest by acquiring a particular shape. Secondly, the cellular sphericity did not present remarkable evolution. Given the variations in the other parameters, this could be due to compensations between opposite effects on this parameter. Thirdly, for the flatness parameter, a decrease of the average values for leaves from 50 to 250 μm of length was observed in a first step. In a second step, for

leaves from 300 to 400 μm , the average value of the flatness increased and beyond 400 μm , it remained stable.

Figure 8 shows histograms of cell orientation. We observed an increase in the number of cells oriented perpendicularly relatively to the leaf surface, thus suggesting an anisotropic directional growth of the cells during the considered leaf developmental stages.

In summary, the variations of the cell parameters over time and throughout leaf surface are indications of the complex and significant morphological evolution of the tissues during leaf morphogenesis and on the onset of cellular groups with a distinct cellular growth pattern.

4.2. Validation of abaxial-adaxial automatic annotation

The proposed method to partition leaf epidermis into abaxial and adaxial cell populations was validated by four biologist experts as described in Sec. 3.3.2. Fig. 9 shows histograms of the classification error rate for our proposed method (algorithm) and the experts. The annotation pro-

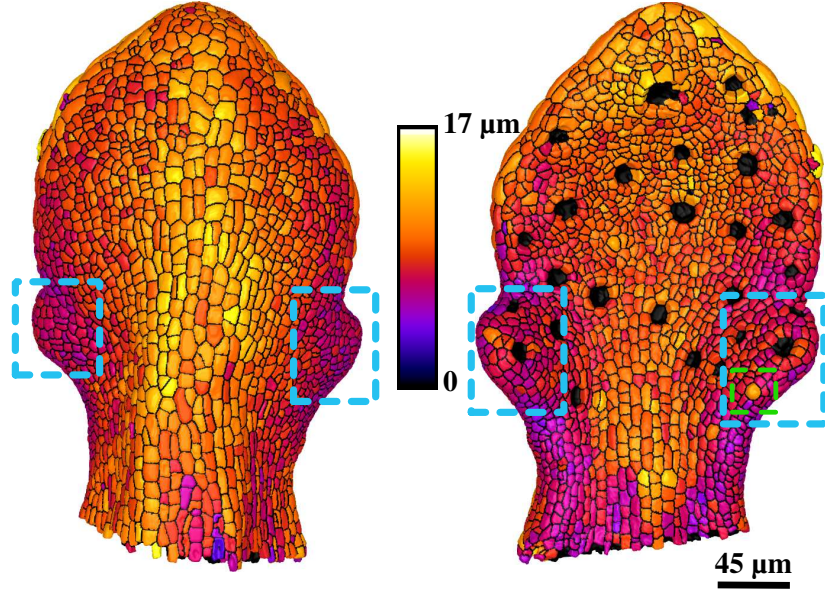


Figure 7: Example of thickness measurement mapped on a 3D leaf surface (leaf 6 Tab.1). *Left*: abaxial side. *Right*: adaxial side. *Blue squares*: leaf teeth. *Green square*: future trichome.

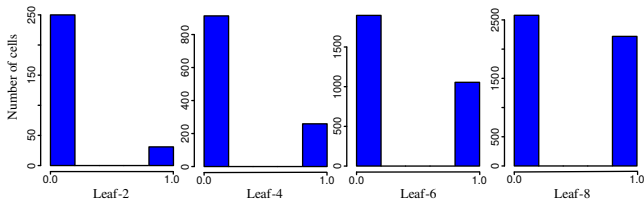


Figure 8: Histograms of cell orientation (*Horizontal axis*: binarized absolute value of the scalar product between cell thickness direction vector and cell major axis).

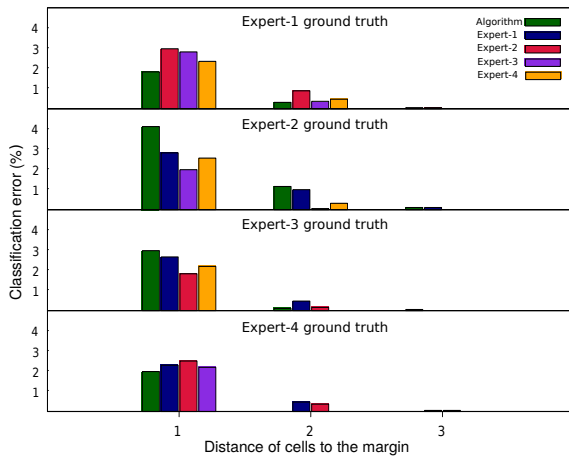


Figure 9: Abaxial-adaxial side segmentation: histograms of cell classification error. *Horizontal axis*: cellular distance to the ground truth margin.

vided by each expert in turn was used as a ground truth. We observed that our proposed method provides the lowest error rate against the other experts regarding the ground truth defined by experts 1 and 4 (respectively 1.82% and 1.94%). For the ground truth defined by experts 2, our method yielded the highest error rate (4.09%), which remains relatively low. Besides, the localization of the separation between abaxial and adaxial sides with our algorithm was generally at most at one cell away from the margin defined by the experts and in only a few cases at two or three cells away. For each expert ground truth, the method provided an error rate comparable to the ones of the other experts. In conclusion, our results suggest that our method performs well for abaxial/adaxial side classification.

4.3. Comparison between abaxial and adaxial sides

Thanks to our proposed method to partition epidermal cells into abaxial and adaxial populations, we were able to quantify the differences of cell morphological parameters between the two sides. Tab. 2 shows the results of the computed cell parameters for 7 leaves by giving the average value and the standard deviation of each parameter. The selected leaves are the same as in Tab. 1 except for leaf 1 that was excluded because its size.

Firstly, we observed that cell volume and elongation in the abaxial population are higher than adaxial one. Secondly, we observed that the difference between the two sides in term of cell number and ECT decreases with time. Thirdly, concerning the flatness and the sphericity parameters, we observed that the average values for the adaxial face

Table 2: Face-specific measurements of morphological 3D cell parameters (average \pm standard-deviation). *Top*: abaxial face. *Bottom*: adaxial face.

Leaves	$L(\mu m)$	Cells	$V(\mu m^3)$	Ψ	E	F	$ECT(\mu m)$
2	72	173	256.67 ± 128.82	0.20 ± 0.04	1.66 ± 0.49	1.25 ± 0.20	6.26 ± 1.52
3	133	456	288.85 ± 163.83	0.19 ± 0.03	1.48 ± 0.39	1.28 ± 0.21	6.61 ± 1.15
4	214	659	296.01 ± 165.57	0.20 ± 0.03	1.47 ± 0.42	1.28 ± 0.21	6.91 ± 1.26
5	222	780	333.73 ± 200.10	0.21 ± 0.04	1.43 ± 0.36	1.28 ± 0.24	7.41 ± 1.34
6	358	1458	349.23 ± 293.71	0.19 ± 0.03	1.38 ± 0.34	1.33 ± 0.25	7.96 ± 2.42
7	428	1829	408.01 ± 397.07	0.20 ± 0.04	1.45 ± 0.56	1.36 ± 0.25	8.46 ± 2.06
8	478	2303	405.60 ± 444.07	0.19 ± 0.03	1.39 ± 0.36	1.39 ± 0.28	8.37 ± 1.67
2	72	108	226.11 ± 128.05	0.22 ± 0.03	1.39 ± 0.28	1.24 ± 0.18	6.54 ± 1.31
3	133	308	221.52 ± 130.02	0.19 ± 0.03	1.37 ± 0.25	1.37 ± 0.27	7.07 ± 1.76
4	214	513	231.29 ± 130.70	0.22 ± 0.03	1.37 ± 0.30	1.36 ± 0.23	7.01 ± 1.37
5	222	620	243.03 ± 168.75	0.20 ± 0.03	1.39 ± 0.29	1.35 ± 0.23	7.47 ± 1.56
6	358	1495	236.46 ± 192.06	0.21 ± 0.03	1.34 ± 0.30	1.40 ± 0.26	7.73 ± 1.47
7	428	1952	262.92 ± 236.88	0.21 ± 0.04	1.37 ± 0.35	1.42 ± 0.27	8.04 ± 1.41
8	478	2494	259.57 ± 245.80	0.20 ± 0.04	1.36 ± 0.34	1.42 ± 0.27	7.85 ± 1.29

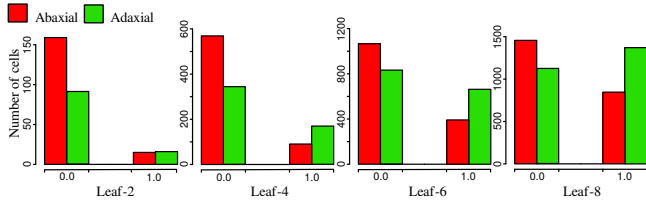


Figure 10: Histograms of cell orientation (*Horizontal axis*: binarized absolute value of the scalar product between cell thickness direction vector and cell major axis). *Red*: abaxial side. *Green*: adaxial side.

are slightly higher than for the abaxial one. Finally, Figure 10 shows histograms of cell orientation for both sides. We observed a higher number of cells oriented perpendicularly to leaf surface in the adaxial side when compared to the abaxial one. This difference increased with leaf length.

To summarize, our results suggest that a large spectrum of differential cellular growth occurs between the two sides during leaf development. This differential growth could participate to the overall evolution of the leaf shape and progressive apparition of blade curvature.

5. Discussion and conclusion

Considering our results, many confirmations and new observations on leaf epidermal cell morphologies have been obtained. However, an in-depth discussion of the biological relevance and implications of these results is out of the scope of the present paper. We discuss here the contributions and the performances of the proposed pipeline for cell shape analysis.

Based on the presented results, it is interesting to note that our pipeline proposes an exhaustive atlas of epidermal cell parameters for leaf morphogenesis quantification. The large amount of computed 3D cell parameters holds great promise for future investigations of organ growth at cellular scale. Our results show that the epidermis of the leaf is composed of a complex cellular organization with variations of cell shape parameters during the development. Furthermore, from the evaluation of the ECT as well as the cellular orientation, we show that the analysis of the leaf cell development should be considered in 3D to systematically capture the spatio-temporal evolution of cell morphology during organ development. Conversely, simplifying cell shapes to 2D could hinder the understanding of leaf morphogenesis. Moreover, thanks to the quantification of the abaxial-adaxial cell shape parameters, we provide a detailed quantitative description of the differential growth between the two sides.

In this work, we developed a framework for 3D leaf epidermal cell shape analysis that allows quantification of 3D cell morphology and its evolution during leaf morphogenesis. This framework was implemented in C++ and the proposed algorithms was integrated in our home made library. The computed cell shape parameters can be mapped on the 3D leaf surface and thus help for the identification of domains with distinct characteristics. The registration and integration of these parametric surface-based representations will provide the basis for developing statistical atlases of leaf morphogenesis. The obtained results can be used for the purpose of quantitative modeling. Last but not least, the various 3D cell parameters that can be computed with our pipeline will also be useful to decipher the development of

other plant organs at the cellular level.

5.0.1 Acknowledgments

This work was supported by the “Institut de Modélisation des Systèmes Vivants” of Idex Paris-Saclay (ANR-11-IDEX-0003-02) (funding to FS). The IJPB benefits from the support of the LabEx Saclay Plant Sciences-SPS (ANR-10-LABX-0040-SPS).

References

- [1] P. Andrey, K. Kiêu, C. Kress, G. Lehmann, L. Tirichine, Z. Liu, E. Biot, P.-G. Adenot, C. Hue-Beauvais, N. Houbahérin, et al. Statistical analysis of 3D images detects regular spatial distributions of centromeres and chromocenters in animal and plant nuclei. *PLoS Comput Biol*, 6(7):e1000853, 2010. [2](#)
- [2] P. Andrey and Y. Maurin. *Free-D*: an integrated environment for three-dimensional reconstruction from serial sections. *Journal of Neuroscience Methods*, 145(1–2):233–244, 2005. [2](#), [4](#)
- [3] L. K. Asl, S. Dhondt, V. Boudolf, G. T. Beemster, T. Beeckman, D. Inzé, W. Govaerts, and L. De Veylder. Model-based analysis of Arabidopsis leaf epidermal cells reveals distinct division and expansion patterns for pavement and guard cells. *Plant Physiology*, 156(4):2172–2183, 2011. [1](#)
- [4] G. W. Bassel and R. S. Smith. Quantifying morphogenesis in plants in 4D. *Current Opinion in Plant Biology*, 29:87–94, 2016. [1](#)
- [5] P. B. de Reuille, A.-L. Routier-Kierzkowska, D. Kierzkowski, G. W. Bassel, T. Schüpbach, G. Tauriello, N. Bajpai, S. Strauss, A. Weber, A. Kiss, et al. Morphographx: a platform for quantifying morphogenesis in 4D. *Elife*, 4:58–64, 2015. [1](#)
- [6] J. Elsner, M. Michalski, and D. Kwiatkowska. Spatiotemporal variation of leaf epidermal cell growth: a quantitative analysis of Arabidopsis thaliana wild-type and triple cyclind3 mutant plants. *Annals of Botany*, 109(5):897–910, 2012. [1](#)
- [7] S. Kalve, D. De Vos, and G. T. Beemster. Leaf development: a cellular perspective. *Frontiers in Plant Science*, 5:362, 2014. [1](#)
- [8] S. Kalve, J. Fotschki, T. Beeckman, K. Vissenberg, and G. T. Beemster. Three-dimensional patterns of cell division and expansion throughout the development of Arabidopsis thaliana leaves. *Journal of Experimental Botany*, page eru358, 2014. [1](#)
- [9] E. Kawamura, G. Horiguchi, and H. Tsukaya. Mechanisms of leaf tooth formation in arabidopsis. *The Plant Journal*, 62(3):429–441, 2010. [1](#)
- [10] L. Liu, E. W. Chambers, D. Letscher, and T. Ju. Extended grassfire transform on medial axes of 2D shapes. *Computer-Aided Design*, 43(11):1496–1505, 2011. [3](#)
- [11] W. E. Lorensen and H. E. Cline. Marching Cubes: A high resolution 3D surface construction algorithm. 21(4):163–169, 1987. [4](#)
- [12] T. D. Montenegro-Johnson, P. Stamm, S. Strauss, A. T. Topham, M. Tsagris, A. T. Wood, R. S. Smith, and G. W. Bassel. Digital single-cell analysis of plant organ development using 3D cell-atlas. *The Plant Cell*, 27(4):1018–1033, 2015. [1](#)
- [13] M. Nakata and K. Okada. The leaf adaxial-abaxial boundary and lamina growth. *Plants*, 2(2):174–202, 2013. [1](#)
- [14] X. Rolland-Nevière, G. Doërr, and P. Alliez. Robust diameter-based thickness estimation of 3D objects. *Graphical Models*, 75(6):279–296, 2013. [3](#)
- [15] T. Schmidt, T. Pasternak, K. Liu, T. Blein, D. Aubry-Hivet, A. Dovzhenko, J. Duerr, W. Teale, F. A. Ditengou, H. Burkhardt, et al. The irocs toolbox–3d analysis of the plant root apical meristem at cellular resolution. *The Plant Journal*, 77(5):806–814, 2014. [2](#)
- [16] H. Silva, S. Sagardia, M. Ortiz, N. Franck, M. Opazo, M. Quiroz, C. Baginsky, and C. Tapia. Relationships between leaf anatomy, morphology, and water use efficiency in aloe vera (l) burm f. as a function of water availability. *Revista Chilena de Historia Natural*, 87(1):1, 2014. [1](#)
- [17] S. Tisné, M. Reymond, D. Vile, J. Fabre, M. Dauzat, M. Koornneef, and C. Granier. Combined genetic and modeling approaches reveal that epidermal cell area and number in leaves are controlled by leaf and plant developmental processes in Arabidopsis. *Plant Physiology*, 148(2):1117–1127, 2008. [3](#)
- [18] E. Truernit, H. Bauby, B. Dubreucq, O. Grandjean, J. Runions, J. Barthélémy, and J.-C. Palauqui. High-resolution whole-mount imaging of three-dimensional tissue organization and gene expression enables the study of phloem development and structure in Arabidopsis. *The Plant Cell*, 20(6):1494–1503, 2008. [2](#)
- [19] J. Weickert. *Anisotropic diffusion in image processing*, volume 1. Teubner Stuttgart, 1998. [2](#)
- [20] N. Wuyts, J.-C. Palauqui, G. Conejero, J.-L. Verdeil, C. Granier, and C. Massonnet. High-contrast three-dimensional imaging of the Arabidopsis leaf enables the analysis of cell dimensions in the epidermis and mesophyll. *Plant Methods*, 6(1):1, 2010. [3](#)
- [21] Y. Yan, K. Sykes, E. Chambers, D. Letscher, and T. Ju. Erosion thickness on medial axes of 3D shapes. *ACM Transactions on Graphics (TOG)*, 35(4):38, 2016. [3](#)